A Modular Platform for Cell Characterization, Handling and Sorting by Dielectrophoresis

S. Burgarella[*,1], B. Dell'Anna[2], V. Perna[2], G. Zarola[2] and S. Merlo[2]
[1]STMicroelectronics, Agrate Brianza (MI), Italy,
[2]Università degli Studi di Pavia, Dipartimento di Elettronica, Pavia, Italy
*Corresponding author: STMicroelectronics, Pal. Fiordaliso, Via C. Olivetti 2, 20041 Agrate Brianza (MI), Italy, email: sarah.burgarella@st.com

Abstract: Dielectrophoresis (DEP) is a method for cell manipulation without physical contact in lab-on-chip devices, since it exploits the dielectric properties of cells suspended in a microfluidic sample, under the action of locally generated high-gradient electric fields. The DEP platform that has been developed offers an integrated solution for customizable applications. Several functional units, organized in a first characterization module and in a series of manipulation stages rearrangeable on a single chip, have been realized using fabrication techniques from micro-electro-mechanical-systems (MEMS) technology. Numerical modelling has been performed using COMSOL Multiphysics to simulate the electric field distribution and to quantify the DEP forces acting at the cell microscale. Parametrical modelling has been performed to optimize the geometry of each module, whose functioning has been demonstrated with different cells types.

Keywords: dielectrophoresis, cell sorting, lab-on-chip, microfluidics, MEMS.

1. Introduction

The physical manipulation of biological cells is of vital importance in the development of miniaturized systems for biological analysis. Precise cell handling is fundamental in microcytometry and cell counting applications; cell manipulation and sorting is also essential in lab-on-chip devices for molecular diagnostics applications, as it represents the preliminary stage of sample preparation, interfacing the clinical sample to the molecular domain [1].

Dielectrophoresis (DEP) is a promising method for cell manipulation in lab-on-chip devices, as it exploits the dielectric properties of cells suspended in a microfluidic sample [2]. High-gradient electric fields are generated by microelectrodes patterned on the silicon substrate of the microfluidic channels using standard fabrication techniques. The modular dielectrophoretic platform that has been developed is composed of several functional units, with different electrode geometries. The characterization modules allow the determination of the dielectric properties of each cell type, while the manipulation stages individually perform basic fluidic unit operations for selective cell filtering, focusing, caging, deviation and concentration. The developed modules can be rearranged on a single chip to assemble application specific systems that can be produced with a standardized, cost-efficient technology, as shown in Figure 1.

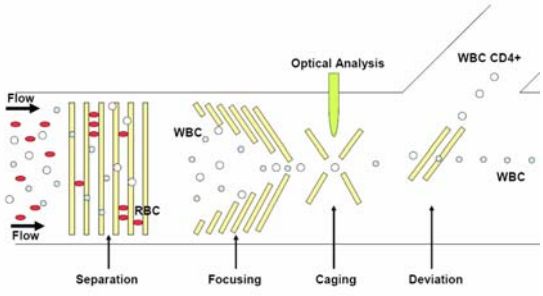

Figure 1. Schematic top view of the microchannel, showing a combination of the developed modules designed to perform a first separation between red blood cells and white blood cells, followed by the sorting of a selected white blood cells subpopulation.

Numerical modelling has been performed using COMSOL Multiphysics to simulate the quasi-static electric field distribution and to quantify the consequent pico-Newton DEP forces acting at the microscale. Suspended cells have been modelled using both a general point-dipole approximation and a more specific 3D geometrical model, considering the dielectric properties of each cell compartment: the cytosol, the membrane and the wall, if present. Parametrical modelling has been performed in order to optimize the geometry of each functional microelectrode module.

Operation and functionality of the single units have been demonstrated with yeast cells and sheep red blood cells. Experimental results were found in agreement with theoretical results obtained using the finite element method.

.

2. Governing Equations

2.1 Point-dipole approximation

When cells are suspended in a spatially non-uniform electric field, a dipole moment is induced in them. If a single cell is modelled as a point-dipole at the spatial position $\overline{r}$, the interaction of the external AC electric field, exhibiting a sinusoidal temporal variation with angular frequency ω, with the induced dipole generates a net time-averaged force composed by two contributions: the DEP force term (1), relative to the in-phase component of the induced dipole moment and the non-uniform field amplitude (Standing Wave Configuration); the Travelling Wave Dielectrophoretic (TWD) force term (2), relative to the out-of-phase component of the induced dipole moment and the non-uniform field-phase [3].

$$\left\langle \overline{F}_{DEP}\left(\overline{r}\right)\right\rangle = 2\pi\varepsilon_m R^3 \,\mathrm{Re}\left(F_{CM}\right)\nabla E_{rms}^2 \qquad (1)$$

$$\left\langle \overline{F}_{TWD}\left(\overline{r}\right)\right\rangle = 2\pi\varepsilon_m R^3 \,\mathrm{Im}\left(F_{CM}\right)\left(E_{x0}^2\nabla\varphi_x + E_{y0}^2\nabla\varphi_y + E_{z0}^2\nabla\varphi_z\right) \qquad (2)$$

In the above formulation, ε_m is the permittivity of the suspending medium, R is the radius of the spherical particle, E_{x0}, E_{y0}, E_{z0} are the magnitudes and φ_x, φ_y, φ_z are the phases of each electric field component and E_{rms} is the root mean square value of the field strength and ∇ is the symbol for gradient. F_{CM} is the Clausius-Mosotti factor, a complex frequency-dependent number calculated accordingly to (3), from the complex permittivities of the medium (ε^*_m), with ohmic conductivity σ_m, and of the cell (ε^*_p), respectively defined by (4) and (5):

$$F_{CM} = \frac{\varepsilon_p^* - \varepsilon_m^*}{\varepsilon_p^* + 2\varepsilon_m^*} \qquad (3)$$

$$\varepsilon_m^* = \varepsilon_m - \frac{j\sigma_m}{\omega} \qquad (4)$$

Eucariotic cells, containing nucleus suspended in a semi-fluid cytosol and enclosed by outer membranes, are modelled as layered spherical particles. For a cell of radius R, with a single outer shell of thickness d, the complex permittivity ε^*_p is given by (5):

$$\varepsilon_p^* = \varepsilon_s^* \left[\frac{\left(\frac{R}{R-d}\right)^3 + 2\left(\frac{\varepsilon_{\mathrm{int}}^* - \varepsilon_s^*}{\varepsilon_{\mathrm{int}}^* + 2\varepsilon_s^*}\right)}{\left(\frac{R}{R-d}\right)^3 - \left(\frac{\varepsilon_{\mathrm{int}}^* - \varepsilon_s^*}{\varepsilon_{\mathrm{int}}^* + 2\varepsilon_s^*}\right)} \right] \qquad (5)$$

where ε^*_s and ε^*_{int} are the complex permittivity of the shell and that of the cell interior, respectively.

The behaviour of cells, suspended in a fluid medium, under the action of the applied electric field, can be deduced by F_{CM}. In particular, the translational movement is related to the real part of F_{CM} (6):

$$\mathrm{Re}\left[F_{CM}\right] = \frac{3\eta U_{particle}}{\varepsilon_m R^2 \nabla E_{rms}^2} \qquad (6)$$

where η is the medium viscosity, R is the particle radius, and $U_{particle}$ is the translational linear velocity. If $\mathrm{Re}[F_{CM}]>0$ cells show a positive response (cells are attracted at the electrodes by a pDEP force), whereas if $\mathrm{Re}[F_{CM}]<0$ cells show a negative behaviour (cells are ejected away from the electrodes by a nDEP force). The rotational movement, which would be induced by the field generated for example in an electrode configuration with a central symmetry as in the case of the quadrupole layout, is related to the imaginary part of F_{CM} (7):

$$\mathrm{Im}\left[F_{CM}\right] = -\frac{2\eta\Omega_{particle}}{\varepsilon_m E_0^2} \qquad (7)$$

where E_0 is the value of the electric field strength and $\Omega_{particle}$ is the rotational velocity in the central position of the quadrupole configuration. Cells move towards regions where the phase of the applied field is larger, if $\mathrm{Im}[F_{CM}]>0$, or smaller, if $\mathrm{Im}[F_{CM}]<0$.

2.2 Geometrical model

An alternative approach consists in considering the real three-dimensional cell geometry and modelling it as a homogeneous sphere with its permittivity and conductivity values. The propagation of the electric field in the volume occupied by the cell lead to the

definition the of electrostatic energy density, according to (8):

$$\rho_E\left(\overline{r}\right)=\frac{1}{2}\varepsilon_0 E^2 \tag{8}$$

where ρ_E is the electrostatic energy per volume unit and E is the value of the electric field in the cell volume. The electrical energy acquired by the cell is given by integrating (8) in its volume, according to (9):

$$U_E=\int_{Volume}\rho_E dV \tag{9}$$

By applying the first derivative of (9) along the three spatial directions, the three components of the dielectrophoretic force can be determined, as shown by equations in (10):

$$F_x=-\frac{\partial U_E}{\partial x}, F_y=-\frac{\partial U_E}{\partial y}, F_z=-\frac{\partial U_E}{\partial z} \tag{10}$$

If compared to the point-dipole approximation, the dielectrophoretic force calculated by applying the geometrical model includes both the force components due to the in-phase and out-of-phase dipole moment. Moreover, it requires a more complex numerical solving: fore these reasons, the point-dipole approximation was mostly preferred in the finite element simulation for the DEP modules.

3. Use of COMSOL Multiphysics

3.1 Characterization stages

As follows from the previous theoretical observations, since the absolute values of the real and imaginary parts of F_{CM} are related, respectively, to the linear and rotational velocity, it is possible to estimate F_{CM}, also for cells with unknown dielectric properties, by means of calculated electric field strengths and experimentally detected velocity values, as highlighted by (6) and (7). This information is essential for an efficient design of the electric excitation to be used in the manipulation stages in order to ensure the desired effect.

The designed characterization modules achieve two different objectives: the two-bar array allows the detection of the translational velocity of the cells and the quadrupole module is used to obtain the rotational velocity of the cells. The microelectrodes of the first module (Figure 2a) are driven with 180° phase-shifted sinusoidal signals. COMSOL Multiphysics has been used to calculate the electric field acting on the cell, while the distribution of the linear velocity as a function of the frequency was experimentally recovered, allowing the determination of Re[F_{CM}] according to (6). In the quadrupole structure (Figure 2b), adjacent electrodes are driven with 90° phase-shifted sinusoidal signals: a time harmonic analysis was performed with COMSOL Multiphysics to calculate the electric field acting at the centre of the structure (Figure 3). The distribution of the rotational velocity, as function of the frequency, was determined for the cells in the centre of the quadrupole, allowing the determination of Im[F_{CM}] according to (7). COMSOL Multiphysics was then used to calculate the dielectrophoretic force acting on the cells, according to the values obtained for F_{CM}. Simulated trajectories and velocities are in agreement to experimental data (Figure 4).

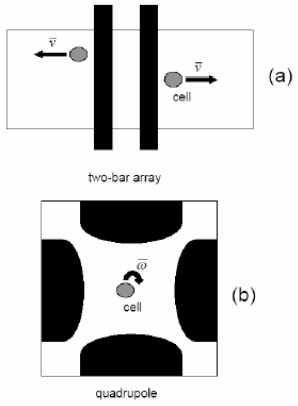

Figure 2. Schematic top view of the characterization modules for Re[F_{CM}] (a) and Im[F_{CM}] (b).

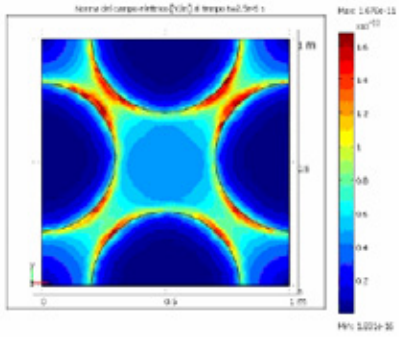

Figure 3. Electric field norm on a surface located 10 µm above the electrodes plane and parallel to it. Voltage signals are 10 Vpp in amplitude, 200 kHz in frequency and 90° phase-shifted.

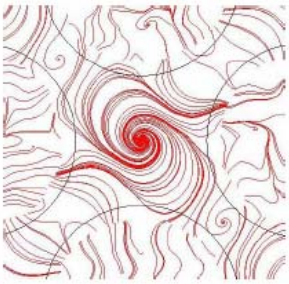

Figure 4. Simulation of *Saccharomyces Cerevisiae* yest cells trajectories in the quadrupole configuration, with applied voltage signals as in Figure 3.

3.2 Manipulation modules

The multi-bar array module (Figure 5a) in composed by bars orthogonally oriented with respect to the axis of the channel and can be used as a selective cell filter, or as a cell conveyer stage, depending on the phase shift between excitations applied to consecutive electrodes. By driving adjacent bars with 180° phase-shifted sinusoidal signals at a selected frequency, two cell types in the same solution can be efficiently separated. Instead, if consecutive electrodes are excited with 90° phase-shifted sinusoidal waves, the overall dielectrophoretic effect is, under nDEP conditions, the levitation of the suspended cells followed by their displacement toward the left or right outlet.

The fishbone-like module (Figure 5b) is an array of parallel bars with different length, oriented at 45° with respect to the channel axis and excited with 90° phase-shifted sinusoids. It acts as a cell focuser, allowing for the alignment of the cell population along the axis of the microfluidic channel.

In the deviation module (Figure 5c), a 45° oriented single-bar electrode on the bottom of the channel is combined with a conductive layer (counter-electrode), realized on the glass cover of the channel, using Indium-Tin Oxide (ITO) to maintain transparency. Exciting these elements with sine waves at 180°, a specific cell type can be deviated along a secondary channel.

The spiral concentration module (Figure 5d) has four parallel spiral electrodes excited with 90° phase-shifted sinusoids: the TWD force acting along the radial direction drives selected cells at the centre of the configuration, allowing direct inspection.

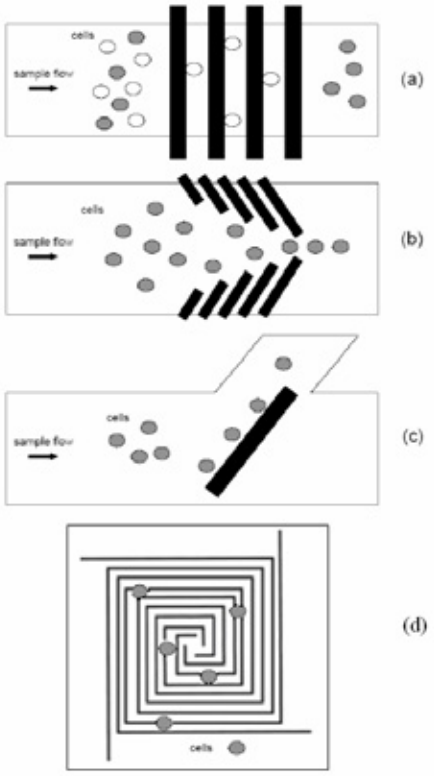

Figure 5. Schematic illustration of multi-bar array (a), fishbone-like focusing module (b), deviation stage (c), and spiral concentrator (d).

Electric field distributions and dielectrophoretic forces acting on the suspended cells were numerically calculated with COMSOL Multiphysics, according to (1) and (2). The proposed electrode geometries were optimized using parametric simulation by interfacing COMSOL Multiphysics with Matlab. Whereas a desired dielectrophoretic effect is obtained by means of a specific electrode geometry, in order to maximize the effect is necessary to study electric field and force trends using parametric simulation. In particular, we have investigated the electrode thickness and separation gap. Thickness was varied from 25 nm to 1 μm with 25-nm steps, while electrode gap was changed from 5 μm to 150 μm with 5-μm steps. Electrode gap and width were assumed to be equal.

In Figure 6 the cross section of parallel bar electrodes patterned on the bottom of the channel and orthogonal to the fluid flow is modelled. The 2-D surface plot shows the electric field magnitude for different

thicknesses: it increases with the electrode thickness, and at the centre of the gap is lower than close to the electrode edges. For fabrication, a 250-nm thickness was selected as a sufficiently high value compatible with the available technology.

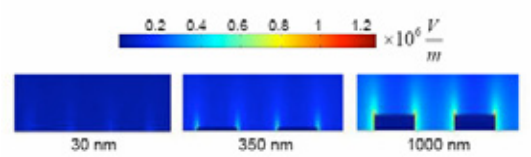

Figure 6. Electric field distribution for different electrode thicknesses (30, 350 and 1000 nm).

Figure 7 show the DEP force as a function of the gap between electrodes. DEP force values depend on the size and on the dielectric properties of the cell under consideration. The DEP force presents a maximum for a gap value of about 50-µm for the cells types of available use in the lab, sheep red blood cells (SRB) and *Saccharomyces Cerevisiae* yest cells. This value was therefore selected for the fabricated units.

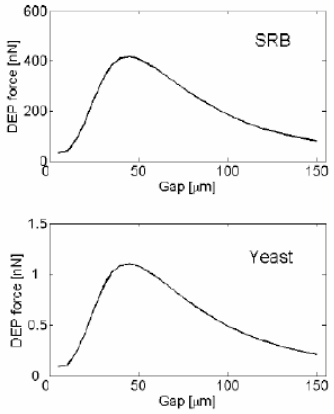

Figure 7. DEP force as a function of the electrode gap for sheep red blood cells (SRB) and *Saccharomyces Cerevisiae* yeast cells suspended in aqueous solution with electrical conductivity of 435 µS/cm.

Action efficiency was also investigated by 3-D multiphysics numerical models, in which fluidodynamic and electrical force components were taken into account. Figure 8a shows the DEP force distribution at the bottom of the microchannel and the particle tracing highlights the focusing effect of the fishbone-like configuration. Figure 8b illustrates the DEP force distribution and the induced effect in the deviation module. Figure 9 shows the electric field acting on the spiral array; streamline indicated the trajectories of cells to the centre of the configuration.

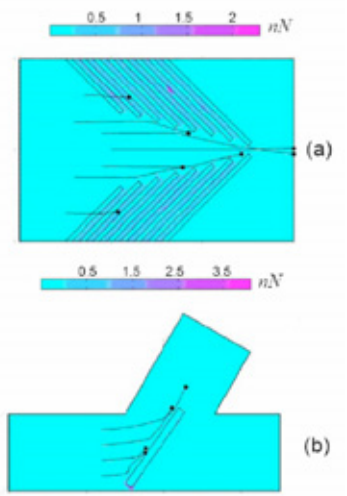

Figure 8. Top view of DEP force distribution and induced effect obtained with 3D models. (a) Fishbone-like configuration with focusing effect on suspended cells; (b) 45° single bar with counter-electrode configuration with deviation effect on suspended cells.

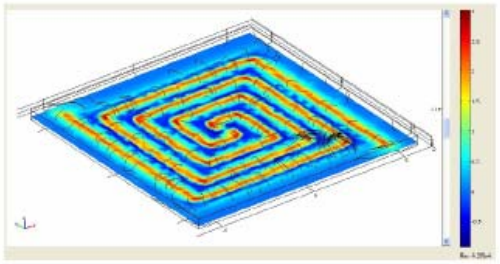

Figure 9. DEP force distribution and cell trajectories for the spiral array concentration module.

4. Experimental Results

4.1 Electrodes fabrication

Gold electrodes were microfabricated with standard lithographic techniques on the silicon substrate of the microchannel. Electrodes consisted of a 250-nm thick metal layer evaporated over a 6 nm Cr seed layer. The electrode width and separation were 50 µm for the two-bar array, multi-bar array, fishbone-like unit and 45° single bar, 20 µm for the spiral array. The quadrupole structure was

arranged as a planar array of semicircular electrodes with 64-µm diameter, separated by 400-µm.

4.2 Dielectric characterization

With 180° phase-shifted sinusoidal signals applied to the parallel bars, cells velocity changed in direction and module with the frequency of the applied signals. For *Saccharomyces Cerevisiae* cells, nDEP was observed from 2 kHz up to 200-300 kHz, since cells were rejected away from the electrodes, while pDEP occurred from 400-500 kHz up to 20 MHz as cells were attracted to the electrodes. For SRB cells, nDEP was observed from 8 kHz to 1 MHz and pDEP from 2 MHz to 8 MHz. Applying 90° phase-shifted sinusoidal signals clockwise to the four electrodes of the quadrupole, counter-clockwise cells electro-rotation was observed for both yeast cells and SRB cells, due to the TWD effect. Figure 10 shows the real and imaginary components of F_{CM} calculated from the measured traslational and rotational velocity and according to (6) and (7), as functions of the applied electric field frequency.

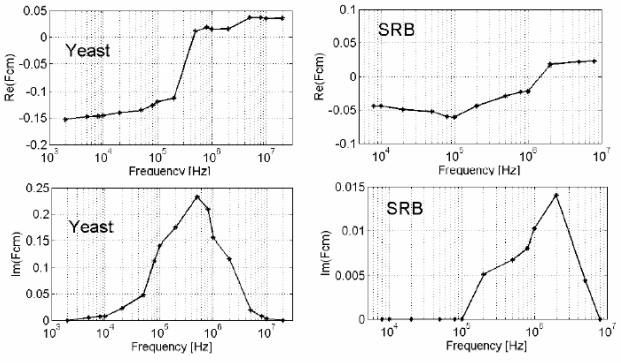

Figure 10. Real and imaginary components of the Clausius-Mosotti factor for yeast cells and SRB cells suspended in aqueous solution with electrical conductivity of 435 µS/cm.

4.3 Cell manipulation

The multi-bar array module allows the sorting of two cellular types if driven at a frequency where one cellular type shows nDEP and the other pDEP. Applying 180° phase-shifted sinusoidal signals to adjacent bars, we noticed that at 1 MHz *Saccharomyces Cerevisiae* yeast cells were trapped in the active zone by pDEP force, while SRB cells were rejected away from the electrodes, as expected from the real part of F_{CM} illustrated in Figure 10. The separation effect is shown in Figure 11: the array filter traps yeast cells at the electrode edges, while SRB cells are levitated and transported by the fluid flow.

The fishbone-like focusing configuration was tested with yeast cells handled through a slow flow of the aqueous solution obtained by capillarity. Using standing wave excitation mode, the most effective frequency value of the applied signals for cell focusing was 500 kHz, while using travelling wave excitation mode was 100 kHz. As can be seen in Figure 12, cells are aligned along the central axis of the microfluidic channel, as expected from the results of the simulations in Figure 8a.

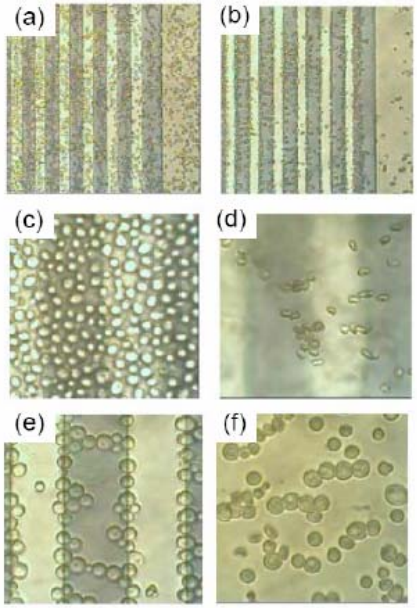

Figure 11. Top view image of cell separation. (a) Electrodes off (10x zoom); (b) Electrodes on (10x zoom); (c) 50x zoom of (a); (d) 50x zoom of (b), highlighting the effect of SRB cells levitation; (e) *Saccharomyces Cerevisiae* cells trapped in the active zone (50x zoom); (f) SRB cells observed far from the active zone at the end of separation process (50x zoom).

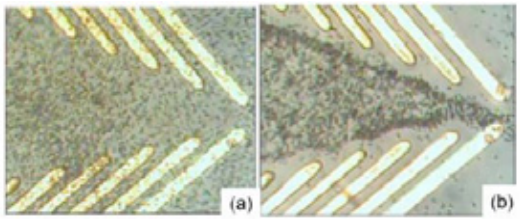

Figure 12. Top view image (5x zoom) of cell focusing effect. (a) Electrodes off; (b) After switching on the electrodes.

The deviation module was tested with yeast cells handled through a slow flow obtained by capillarity. Applying 180° phase-shifted sinusoidal signals to a 45° single electrode and counter-electrode, the most effective frequency value of the applied signals for the cell deviation was 200 kHz. The effect is shown in Figure 13.

The spiral array module was similarly tested for concentrating yeast cells at the centre of the configuration by applying 90° phase-shifted voltage sinusoids at the electrodes, as shown in Figure 14.

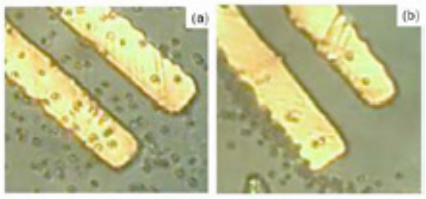

Figure 13. Top view image (10x zoom) of the effect of cell deviation. (a) Electrode off; (b) only one 45° electrode switched on for cells deviation.

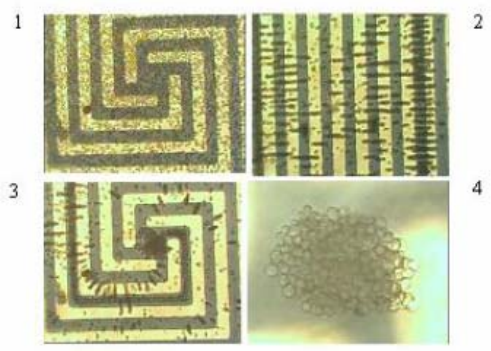

Figure 14. Progressive yeast cell concentration at the centre of the spiral array by TWD force (top view).

5. Conclusions

Different modular dielectrophoretic elements have been individually analyzed in order to obtain a multi-functional system. The developed platform is composed of several functional units, organized in characterization stages and in a series of manipulation modules. Modules were designed, simulated, fabricated and tested using *Saccharomyces Cerevisiae* yeast cells and SRB cells. Experimental results were found in agreement with performed numerical finite element simulations. These modules were successfully used to characterize the two cellular types used in this work, allowing the estimation of F_{CM} as a function of the frequency and, consequently, the prediction of the cell behaviour under the action of a non-uniform electric field. Cells were also separated with a multi-bar array module and manipulated with a fishbone-like structure, a deviation module and a spiral array concentrator.

The followed approach allows design and fabrication of application specific systems by easily combining various dielectrophoretic modules, electrically independent of each other, since microparticles or biological cells can be carried on from one module to another by flow. The presented integration of different dielectrophoretic elements opens up new possibilities for miniaturized particle or cell counters and flow cytometers. Complete miniaturized processing and analysis systems could be produced in the future on a chip, with ready off-the-shelf components.

6. References

1. Huang Y et al., “Electric manipulation of bioparticles and macromolecules on microfabricated electrodes”, *Anal Chem*., **73**, 1549-59, 2001

2. Fu LM et al., “Manipulation of microparticles using new modes of traveling-wave-dielectrophoretic forces: numerical simulation and experiments”, *IEEE/ASME Transaction on Mechatronics*, **9-2**, 377-83, 2004

3. Jones TB., “Basic theory of dielectrophoresis and electrorotation”, *Engineering in Medicine and Biology Magazine, IEEE*, **22-6**, 33-42, 2003